New Journal of Physics

Entanglement-assisted atomic clock beyond the projection noise limit

Anne Louchet-Chauvet[1], Jürgen Appel, Jelmer J Renema, Daniel Oblak, Niels Kjaergaard[2] and Eugene S Polzik[3]

QUANTOP, Niels Bohr Institute, University of Copenhagen, Blegdamsvej 17, 2100 København Ø, Denmark
E-mail: polzik@nbi.dk

Abstract. We use a quantum non-demolition measurement to generate a spin squeezed state and to create entanglement in a cloud of 10^5 cold cesium atoms. For the first time we operate an atomic clock improved by spin squeezing beyond the projection noise limit in a proof-of-principle experiment. For a clock-interrogation time of $10\,\mu$s, the experiments show an improvement of 1.1 dB in the signal-to-noise ratio, compared to the atomic projection noise limit.

[1] Present address: LNE-SYRTE, Observatoire de Paris, CNRS, UPMC, 61 avenue de l'Observatoire, 75014 Paris, France.
[2] Present address: Danish Fundamental Metrology, Matematiktorvet 307, 2800 Kgs-Lyngby, Denmark.
[3] Author to whom any correspondence should be addressed.

IOP Institute of Physics ⏀ DEUTSCHE PHYSIKALISCHE GESELLSCHAFT

Contents

1. Introduction

Atomic projection noise, originating from the Heisenberg uncertainty principle, is a fundamental limit to the precision of spectroscopic measurements when dealing with ensembles of independent atoms. This limit has been approached, for example, in atomic clocks [1]–[3]. Theoretical studies have shown that introducing quantum correlations between the atoms can help to overcome this limit and reach even better precision [4]–[8]. Spin squeezing in a system of two ions has been shown to improve the precision of Ramsey spectroscopy for frequency measurements [9]. Furthermore, squeezed atomic ensembles improve the sensitivity of magnetometers [10, 11].

In a previous publication [12], we reported the generation of quantum noise squeezing on the cesium clock transition via quantum non-demolition (QND) measurements. By proposing an entanglement-assisted Ramsey (EAR) method including a QND measurement, we showed how this squeezing could help to improve the precision of atomic clocks. In this work, we describe the spin squeezing experiment in more detail and implement the complete EAR clock sequence. For the first time, we demonstrate an atomic microwave clock improved by spin squeezing. Decoherence effects are measured and included in the analysis. The clock reported here does not reach record precision due to technical reasons; however, the demonstrated approach is applicable to the state-of-the-art clocks, as indicated in [13].

IOP Institute of Physics **ΦΦ** DEUTSCHE PHYSIKALISCHE GESELLSCHAFT

2. Generation of a conditionally squeezed atomic state

2.1. Coherent and squeezed spin states

An ensemble of N_A identical 2-level atoms can be described as an ensemble of pseudo-spin-1/2 particles. We define the collective pseudo-spin vector $\hat{J}$ as the sum of all individual spins. Traditionally, its z-component J_z is defined by the population difference ΔN, such that $J_z = \frac{1}{2}(N_\uparrow - N_\downarrow) = \Delta N/2$. A coherent spin state (CSS) is a product state (i.e. atoms are uncorrelated) where the spins of N_A atoms are aligned in the same direction, for example such that $J_x = N_A/2$, i.e. $|\text{CSS}\rangle = \bigotimes_{i=1}^{N_A} \frac{1}{\sqrt{2}}(|\uparrow\rangle_i + |\downarrow\rangle_i)$. Then, the other projections of $\hat{J}$ minimize the Heisenberg uncertainty relation: $\text{var}(J_z) \cdot \text{var}(J_y) \geqslant \langle J_x \rangle^2/4$ and $\text{var}(J_z) = \text{var}(J_y) = N_A/4$. These quantum fluctuations, referred to as *CSS projection noise*, pose a fundamental limit to the precision of the J_z measurement [14]. It is possible to reduce the fluctuations of one of the spin components—for example J_z—to below the projection noise limit by introducing quantum correlations between different atoms within the atomic ensemble. In this case, the fluctuations on the conjugate observable—here J_y—increase according to the Heisenberg uncertainty relation. Such a state is referred to as a spin squeezed state (SSS). Whether the atoms exhibit non-classical correlations is determined by the criterion

$$\text{var}(J_z) < \frac{\langle J \rangle^2}{N_A} \quad \Leftrightarrow \quad \xi = \frac{\text{var}(J_z)}{\langle J \rangle^2} N_A < 1, \tag{1}$$

where ξ is called the squeezing parameter. Under this condition (even for a general mixed state) the atoms are entangled whereby the signal-to-projection-noise ratio in spectroscopy and metrology experiments is improved by a factor of $1/\xi$ in variance, or $1/\sqrt{\xi}$ in standard deviation [4]. Equation (1) will be referred to as the Wineland criterion throughout this paper.

Spin squeezing can be produced, for example, by atomic interactions [15, 16], by mapping the properties of squeezed light onto an atomic ensemble [17]–[20] or by non-destructive measurements on the atoms [21]–[27]. We follow the last approach by performing a weak, non-destructive measurement of the J_z spin component. Any later measurement on J_z on the same ensemble will be partly correlated to the first measurement outcome. Therefore, the outcome of a subsequent J_z-measurement can be predicted to a precision better than the CSS-projection noise. In other words, if ϕ_1 and ϕ_2 are the outcomes of the first and second measurements, respectively, the conditional variance $\text{var}(\phi_2 - \zeta\phi_1)$ is reduced to below the variance of a single measurement $\text{var}(\phi_1) = \text{var}(\phi_2)$, where ζ is the correlation strength $\zeta \equiv \text{cov}(\phi_1, \phi_2)/\text{var}(\phi_1)$. If the QND measurement does not reduce the length of the pseudo-spin vector $\langle J \rangle$ too much, equation (1) implies that the reduction of the variance results in a metrologically relevant SSS.

2.2. Preparation of the coherent spin state

The experimental sequence for the preparation of the CSS and the QND measurements is shown in figure 1. Cesium atoms are first loaded from a background cesium vapor into a standard magneto-optical trap (MOT) on the D_2-line, and are then transferred into an elongated far off-resonant dipole trap. The dipole trap is generated by a Versadisk laser with a wavelength of 1032 nm and a power of 2.3 W, which is focused to a 20 μm radius spot to confine an elongated atomic sample. After the loading of the dipole trap, the MOT is switched off and a bias magnetic field is applied, defining a quantization axis orthogonal to the trapping beam.
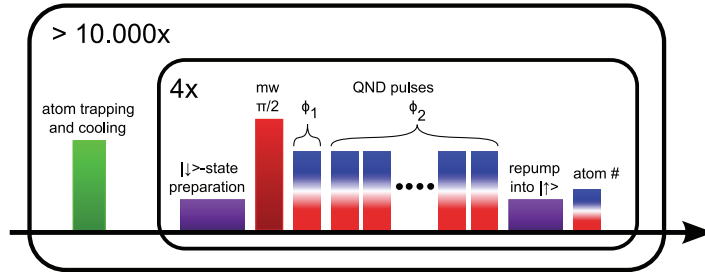
Figure 1. Experimental pulse sequence for the preparation of a CSS and QND measurements.

The $6S_{1/2}|F = 3, m_\mathrm{F} = 0\rangle$ and $6S_{1/2}|F = 4, m_\mathrm{F} = 0\rangle$ ground levels are referred to as the *clock levels*. We denote them as $|\downarrow\rangle$ and $|\uparrow\rangle$, respectively. The cesium atoms are then prepared in the clock level $|\downarrow\rangle$ by optical pumping. Atoms remaining in states other than $|\downarrow\rangle$ due to imperfect optical pumping are subsequently pushed out of the trap, as described in [12]. A resonant microwave pulse ($\pi/2$-pulse) is used to put the atoms into $|CSS\rangle$. We then perform successive QND measurements of the atomic population difference ΔN by detecting the state-dependent phase shift of probe light pulses with a Mach–Zehnder interferometer, as described in detail in section 2.3. Later on, we optically pump the atoms into $F = 4$ to measure the atom number N_A. We recycle the remaining atoms for three subsequent experiments, preparing them into a CSS, performing successive QND measurements and finally measuring the atom number. After these four experiments, all the atoms are blown away with laser light and we perform three series of QND measurements with the empty interferometer to obtain a zero phase shift reference measurement. This sequence is repeated several thousand times with a cycle time of $\approx 5\,\mathrm{s}$.

To ensure that the microwave does not address hyperfine transitions other than the clock transition, the bias magnetic field B is set so that the Zeeman splitting ΔE_Z between adjacent magnetic sublevels ($350\,\mathrm{kHz\,G^{-1}}$ to first order) coincides with one of the zeroes of the microwave pulses' frequency spectrum: $\Delta E_\mathrm{Z} = \ell/\tau_{\pi/2}$, where $\tau_{\pi/2}$ is the microwave $\pi/2$ pulse duration and ℓ is an integer number. Therefore, for typical durations of $\tau_{\pi/2} = 7\,\mu\mathrm{s}$, we set the bias magnetic field to $1.22\,\mathrm{G}$.

2.3. Dispersive population measurement

In order to measure an atomic squeezed state, we require a measurement sensitivity that is sufficient to reveal the atomic projection noise limit. The population in each clock level is measured via the phase shift imprinted on a dual-color beam propagating through the atomic cloud [28]. The dipole trap overlaps with one arm of a Mach–Zehnder interferometer (see figure 2). A beam $P_\downarrow$ of one color off-resonantly probes the $|F = 3\rangle \rightarrow |F' = 2\rangle$ transition, whereas a second beam $P_\uparrow$ off-resonantly probes the $|F = 4\rangle \rightarrow |F' = 5\rangle$ transition (see figure 3). Each color experiences a phase shift proportional to the number of atoms in the ground state of the probed transition: $\phi_\downarrow = \chi_\downarrow N_\downarrow$ and $\phi_\uparrow = \chi_\uparrow N_\uparrow$ [29]. We carefully choose the probe detunings to ensure that the coupling constants are equal: $\chi_\uparrow = \chi_\downarrow$. The two probe beams emerge from one single-mode polarization maintaining fiber, and their intensities are stabilized to be equal $n_\uparrow = n_\downarrow$ to within 0.1%.
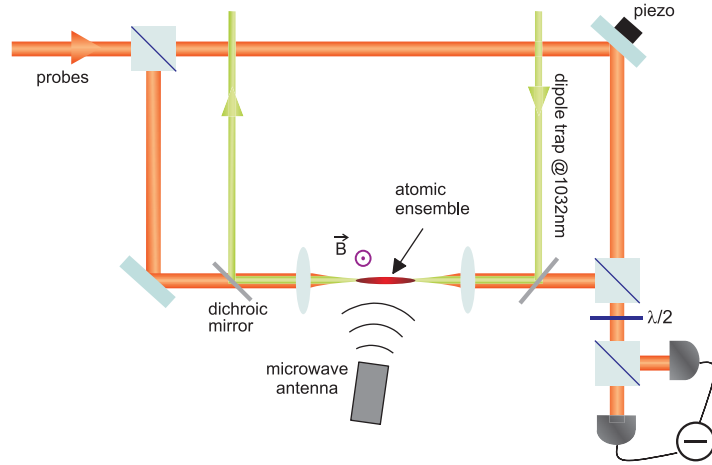
Figure 2. The Mach–Zehnder interferometer. The atoms are placed in one arm of a Mach–Zehnder interferometer. The dipole trapping beam overlaps with the probe arm to form an elongated atomic cloud along the propagation direction of the probe beam. Two probe beams of identical linear polarization enter the interferometer via the same input port and acquire phase shifts proportional to the number of atoms in the clock states $N_\uparrow$ and $N_\downarrow$, respectively. The bias magnetic field (B) is aligned to the polarization of the probe beams.
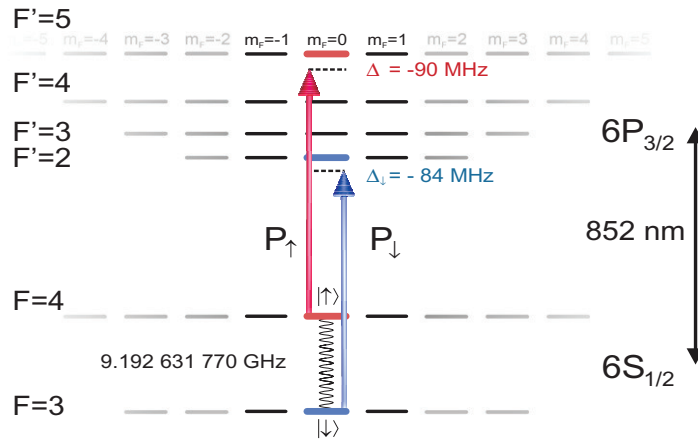

Figure 3. Cesium D_2-line level diagram.

For each individual probe, the photocurrent difference between the detectors at the two output ports of the interferometer reads as

$$\Delta n_\uparrow = n_\uparrow \beta \cos(k_\uparrow \Delta L + \chi_\uparrow N_\uparrow) \quad \text{and} \quad \Delta n_\downarrow = n_\downarrow \beta \cos(k_\downarrow \Delta L + \chi_\downarrow N_\downarrow), \quad (2)$$

where $k_\uparrow$ and $k_\downarrow$ are the wave vector lengths for $P_\uparrow$ and $P_\downarrow$, respectively, ΔL is the interferometer path length difference and $\beta = \sqrt{13}$ is the ratio of the field amplitudes in the reference- and probe-arm of the interferometer. In the absence of atoms $N_\uparrow = N_\downarrow = 0$; therefore the smallest interferometer path length difference that leads to opposite phase for the signals $\Delta n_\uparrow$ and $\Delta n_\downarrow$ is $\Delta L_0 = \pi/(k_\uparrow - k_\downarrow)$. Since the wavelengths of the two probe lasers are so close (to one part in 40 000), one can assume that the fringes of each color are of opposite phase in the

neighborhood of several wavelengths around ΔL_0. The interferometer path length difference[4] is set to the value closest to ΔL_0 that also satisfies $\Delta n_\uparrow = \Delta n_\downarrow = 0$. This path length difference therefore varies with the expected atom number. To account for technical imperfections in the balancing of the probe powers and frequencies, we define the average effective coupling strength $n\chi \equiv (n_\uparrow \chi_\uparrow + n_\downarrow \chi_\downarrow)/2$ and the balancing error $n\Delta\chi \equiv (n_\uparrow \chi_\uparrow - n_\downarrow \chi_\downarrow)/2$ as well as the average intensity $n = (n_\uparrow + n_\downarrow)/2$.

This way, the total photocurrent difference $\Delta n = \Delta n_\uparrow + \Delta n_\downarrow$ reads

$$\Delta n = n_\uparrow \beta \sin(\chi_\uparrow N_\uparrow) - n_\downarrow \beta \sin(\chi_\downarrow N_\downarrow) \simeq n\beta(\chi \, \Delta N + \Delta\chi \, N_A). \tag{3}$$

We define the phase measurement outcome as

$$\phi \equiv \frac{\Delta n}{\beta n} = \frac{\delta n}{\beta n} + \chi \, \Delta N + \Delta\chi \, N_A, \tag{4}$$

where δn denotes the total shot noise contribution from both colors. The phase ϕ provides a measurement of ΔN with added shot noise and classical noise. For N_A atoms in a CSS, we have $\mathrm{var}(\Delta N) = N_A$. The projection noise increases with the atom number and, using $\langle \Delta\chi \rangle = 0$, $\langle \Delta N \rangle = 0$, we obtain

$$\mathrm{var}(\phi) = \frac{\beta^2 + 1}{2\beta^2}\frac{1}{n} + \chi^2 N_A + \mathrm{var}(\Delta\chi) \, N_A^2. \tag{5}$$

After each experiment we use the same dual-color probe beam to determine the total atom number N_A. To this end, we first optically pump all atoms into $|F = 4, m_F = -1, 0, +1\rangle$. The phase measurement outcome reads as $\phi = n\bar{\chi} N_A$, where $\bar{\chi}$ is the effective coupling constant for the probe $P_\uparrow$ when the atoms are distributed among different magnetic sublevels. The similarity of the Clebsch–Gordan coefficients for the $|F = 4, m_F\rangle \rightarrow |F' = 5, m_F\rangle$ transitions (with low $|m_F|$) ensures that $\bar{\chi} \approx \chi$, which is confirmed by experiments with a precision of better than 5%.

2.4. Projection noise measurements

The two probe beams are generated by two extended-cavity diode lasers, which are phase locked in order to minimize their relative frequency noise [30]. Their detunings are given in figure 3.

In figure 4, we analyze the variance of the atomic population difference measurement as a function of the atom number.

As the data acquisition proceeds over several hours, it is a major challenge to keep experimental parameters, such as $\tau_{\pi/2}$, constant to much better than $1/\sqrt{N_A}$ so that the mean values of the atomic population difference measurements does not drift by more than their quantum projection noise. To eliminate the influence of such slow drifts, we subtract the outcomes of measurements performed on independent atomic ensembles recorded in successive MOT cycles from each other. We then calculate the variances using these differential data.

The correlated and uncorrelated parts of the noise variance are fitted with second order polynomials. According to equation (5), we interpret the linear part of this fit as the CSS

---

[4] In [12], we used opposite input ports for the two probe colors and operated the interferometer in its white-light position $\Delta L = 0$ to minimize sensitivity to differential probe frequency noise. The method described here allows us to feed light of both probe colors into the interferometer through one common single mode fiber. This eliminates a possible spatial mode mismatch, which leads to spatially inhomogeneous differential ac-Stark shifts across the atomic sample. The differential probe frequency is controlled tightly using an optical phase lock [30].
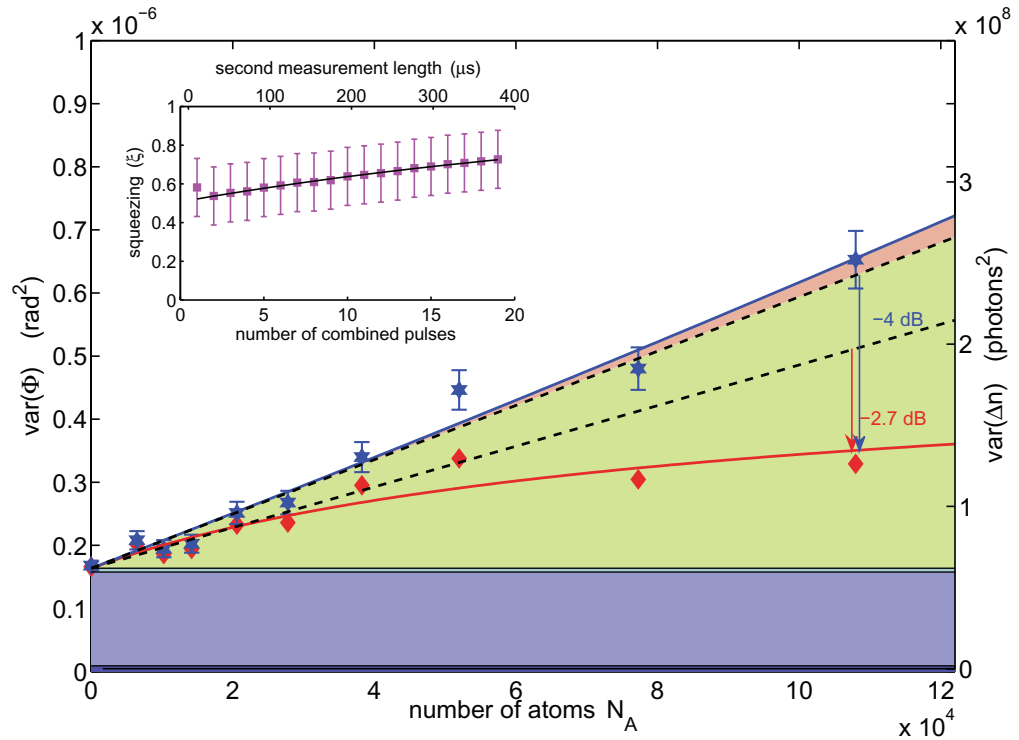
Figure 4. Projection noise and spin squeezing. The first QND measurement is performed with a $10\,\mu s$ bichromatic pulse containing 6×10^6 photons in total. The second measurement comprises two such pulses. Blue stars: variance of the second measurement $\mathrm{var}(\phi_2)$, where the data are sorted by atom number and grouped into ten bins. Solid blue line: quadratic fit to $\mathrm{var}(\phi_2)$. Green area: atomic projection noise of the CSS. Red diamonds: conditional variance $\mathrm{var}(\phi_2 - \zeta\phi_1)$. Red line: reduced noise as predicted by the fits to the noise data. The error bars correspond to the statistical uncertainty given by the number of measurements. These data are obtained by acquiring 1200 MOT loading cycles, i.e. 4800 experiments. Inset: metrologically relevant spin squeezing ξ (as defined in equation (1)) as a function of the number of pulses combined to form the second measurement. The data are fitted with an exponential decay (solid line).

projection noise contribution. We observe a negligible quadratic part, which means that classical noise sources, like laser intensity and frequency fluctuations, which cause noise in the effective coupling constant, are small. Achieving this linear noise scaling is a significant experimental challenge (see [12, Suppl.]), since the effect on ΔN of various sources of classical noise must be kept well below the level of $1/\sqrt{N_A} \simeq 3 \times 10^{-3}$ between independent measurements, i.e. for a duration of $\simeq 5$ s.

2.5. Conditional noise reduction

Both measurements ϕ_1 and ϕ_2 are randomly normally distributed around zero with variances that have contributions from the shot noise and the atomic projection noise:

$$\mathrm{var}(\phi_1) = \frac{1}{n_1} + \chi^2 N_A, \quad \mathrm{var}(\phi_2) = \frac{1}{n_2} + \chi^2 N_A. \tag{6}$$

Since the two measurements are performed on the same atomic sample, they are correlated: $\mathrm{cov}(\phi_1, \phi_2) = \chi^2 N_A$. The conditional variance $\mathrm{var}(\phi_2 - \zeta\phi_1)$ is minimal when $\zeta = \frac{\mathrm{cov}(\phi_1,\phi_2)}{\mathrm{var}(\phi_1)}$:

$$\mathrm{var}(\phi_2 - \zeta\phi_1) = \frac{1}{n_2} + \frac{1}{1+\kappa^2}\chi^2 N_A. \tag{7}$$

We measure $\kappa^2 = 1.6$ for $N_A = 1.2 \times 10^5$ atoms and we obtain a reduction of the projection noise by $\frac{1}{1+\kappa^2} = -4\,\mathrm{dB}$ compared to the CSS projection noise, as indicated by the blue arrow in figure 4.

2.6. Decoherence

Dispersive coupling is inevitably accompanied by spontaneous photon scattering, inducing atomic population redistribution among the ground magnetic sublevels, as well as a reduction of coherence between the clock levels. Due to the selection rules, the population redistribution predominantly occurs within the Zeeman structure of the hyperfine levels [28]: atoms that scatter a photon from the $P_\downarrow$ probe almost certainly end up in the $|F = 3, m_F = -1, 0, +1\rangle$ sublevels again, and atoms that scatter a photon from the $P_\uparrow$ probe predominantly end up in the $|F = 4, m_F = -1, 0, +1\rangle$ states (see figure 3). More importantly, the similarity of the Clebsch–Gordan coefficients that describe coupling of the probe light to low $|m_F|$-sublevel states ensures that the optical phase shift is almost unaffected by such a population redistribution. This makes our dual-color measurement an almost ideal QND measurement as spontaneous scattering events effectively do not change the outcome of a J_z measurement, i.e. no extra projection noise due to repartition into the opposite hyperfine ground states is added. On the other hand, the spontaneous photon scattering still leads to a shortening of the mean collective spin vector $\langle J \rangle \to (1 - \eta)\langle J \rangle$.

The photon number dependence of this mechanism can be modeled as $\eta = 1 - \mathrm{e}^{\alpha n}$, where n is the total number of photons in the probe pulse. We measure the parameter α in a separate experiment, by comparing the Ramsey fringe amplitudes with and without a bichromatic QND pulse between the two microwave $\pi/2$-pulses, as shown in figure 5. We obtain a value of $\alpha = -2.39 \times 10^{-8}$ for this particular atomic cloud geometry and probe detuning.

Each probe color induces an inhomogeneous ac-Stark shift on the atomic levels, causing additional dephasing and decoherence. Nevertheless, in our two-color probing scheme, the Stark shift on level $|\uparrow\rangle$ caused by probe $P_\uparrow$ is compensated by an identical Stark shift on level $|\downarrow\rangle$ caused by probe $P_\downarrow$, provided that the probe frequencies are set so that $\chi_\uparrow = \chi_\downarrow$ and the probe powers are equal. Hence, the two Ramsey fringes depicted in figure 5 (with and without a light pulse) are in phase to better than $1°$.

2.7. Squeezing and entanglement

A QND measurement is characterized by the decoherence η it induces, and by the κ^2-coefficient that describes the measurement strength. In the absence of classical noise, for the dual-color QND the squeezing parameter as defined in equation (1) can be written as

$$\xi_{\mathrm{lin}} = \frac{1}{(1-\eta)^2(1+\kappa^2)}. \tag{8}$$

Therefore, for a fixed detuning of the laser frequencies, the choice of the number of photons used in a QND measurement is the result of a trade-off between the amount of decoherence induced by the photons and the amount of information that the ϕ_1-measurement yields [31].
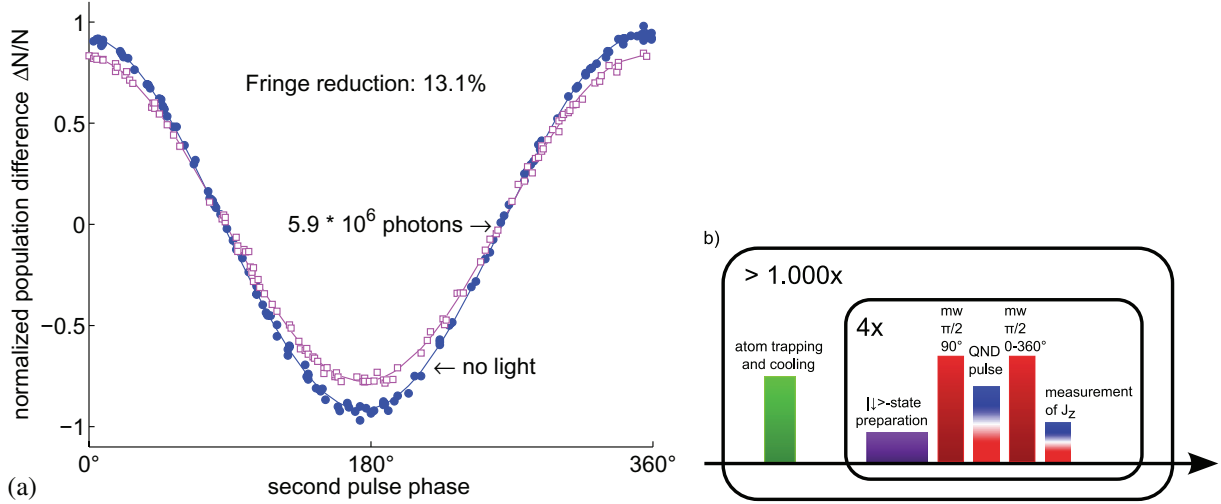
Figure 5. Decoherence measurement via Ramsey fringe reduction. (a) Closed circles: full Ramsey fringe. Open squares: reduced fringe when a QND pulse containing 5.9×10^6 photons is inserted in the Ramsey sequence. In this experiment, the fringe height is reduced by 13.1%, leading to a decoherence parameter $\alpha = 2.39 \times 10^{-8}$. (b) Pulse sequence.

Here, we use $n_1/2 = 3 \times 10^6$ photons per probe color, inducing a shortening of $\eta = 14\%$ of the collective spin J. From equation (8) we expect an improvement of the signal-to-projection-noise ratio by $1/\xi_{\text{lin}} = 2.8\,\text{dB}$ compared to a CSS. From the data presented in figure 4 we measure $1/\xi = 2.7\,\text{dB}$, as indicated with a red arrow. This value agrees well with the theory and with the results reported in [12].

The detuning of the probe light with respect to the atomic transitions (see figure 3), as well as the duration of the probe pulses ($10\,\mu\text{s}$), have been chosen to minimize the influence of classical noise sources, such as electronic noise in the detector and relative frequency- and intensity-noise of the two probe colors.

Since the probe pulses redistribute population only within the hyperfine manifold (cf section 2.6), the light shot noise contribution in the second measurement variance can be reduced by increasing the number of photons n_2 in the second measurement (cf equation (8)). In our experiment, the second measurement comprises several $10\,\mu\text{s}$ long bichromatic pulses containing a total of n_2 photons, separated by $10\,\mu\text{s}$. As shown in the inset of figure 4, ξ exponentially approaches unity as more pulses are combined to form the second measurement. We attribute this decay to the atomic motion within the dipole trap during the second measurement: the atoms move in the transverse profile of the probe beam and are probed with a position-dependent weight corresponding to the local probe light intensity. Movement during the time interval between the first and second probe pulses therefore induces a decay of the correlations between the two measurements. We fit the experimental data with

$$\xi(t_2) = 1 - B\,e^{-t_2/\tau_{\text{decay}}}, \tag{9}$$

where t_2 is the total duration of the second measurement, and obtain $\tau_{\text{decay}} = 670\,\mu\text{s}$, which is of the same order of magnitude as half the radial trap oscillation period [32].
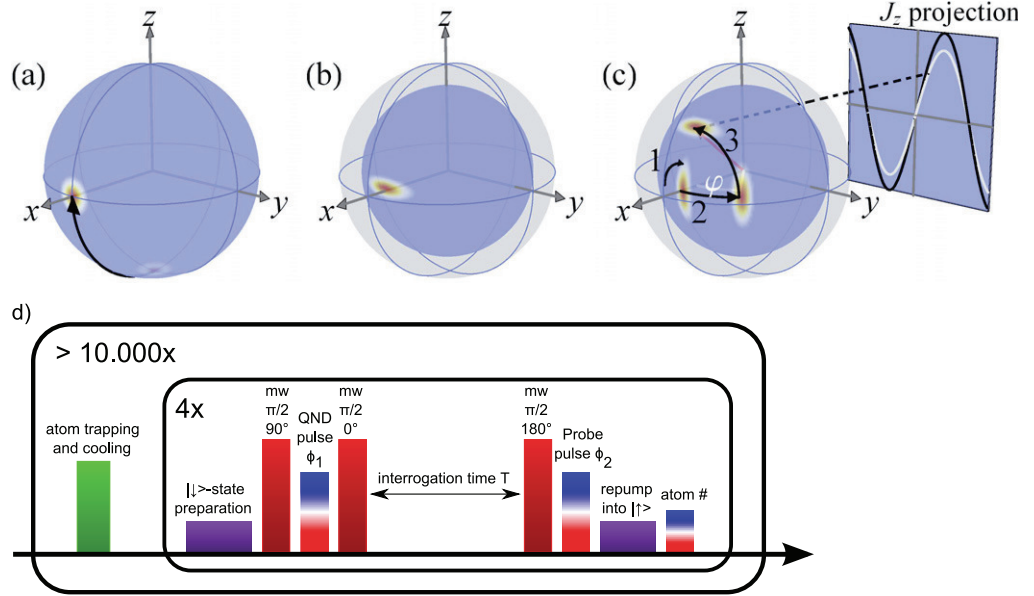
Figure 6. Ramsey sequence including squeezing in the Bloch sphere representation. The sequence starts with all atoms in $|\downarrow\rangle$. (a) A near-resonant $\pi/2$-pulse is applied with phase $\vartheta_0 = 90°$, placing the atoms in a CSS along the x-axis. (b) The atomic state is squeezed along the z-direction by a weak QND measurement of the population difference. The decoherence induced by the first QND measurement leads to a reduction of the Bloch sphere radius. (c.1) A second $\pi/2$-pulse with phase $\vartheta_1 = 0°$ rotates the atomic state around the x-axis, thus converting the population squeezing into phase squeezing. (c.2) Free precession during interrogation time T, equivalent to a rotation around the z-axis by an angle $\varphi = \Delta T$. (c.3) A third $\pi/2$-pulse, with phase $\vartheta_2 = 180°$, acts as a $\pi/2$-rotation around the x-axis. The final state has a z-axis component $\langle J_z \rangle = (1 - \eta)(N_A/2)\sin\varphi$. The reduction of the atomic projection noise results in a reduced uncertainty in the measurement of ϕ_2. (d) Diagram of the pulse sequence.

3. Entanglement-assisted atomic clock

3.1. Entanglement-assisted Ramsey sequence

We use the spin squeezing technique described in the previous section to improve the precision of a Ramsey clock. The modified Ramsey sequence is shown in figure 6. As in a traditional Ramsey sequence, all atoms are prepared in $|\downarrow\rangle$ initially. A near-resonant $\pi/2$-pulse with a phase of $\vartheta_0 = 90°$ and detuning Δ drives them into a CSS with macroscopic $J_x = \frac{N_A}{2}$ (figure 6(a)). This state is then squeezed along the z-direction by performing a weak QND measurement of the pseudo-spin component J_z (figure 6(b)). This population-squeezed state is converted into a phase-squeezed state by a second $\pi/2$-pulse with phase $\vartheta_1 = 0°$ that rotates the state around the x-axis. At this point, the Ramsey interrogation time starts (figure 6(c.1)). We let the atoms evolve freely for a time T, during which they acquire a phase proportional to the microwave detuning $\varphi = \Delta T$ (figure 6(c.2)). To stop the clock, a third $\pi/2$-pulse with phase

$180°$ is applied, converting the accumulated atomic phase shift φ into a population difference (figure 6(c.3)). Finally, we measure the J_z-spin component a second time and from the two measurement outcomes we compute the conditional variance $\mathrm{var}(\phi_2 - \zeta\phi_1)$.

The first QND measurement of J_z shown in figure 6(b) induces decoherence that reduces the pseudo-spin vector length, and hence the Ramsey fringe height, so that

$$\langle J_z \rangle = (1 - \eta)\frac{N_A}{2}\sin\varphi, \tag{10}$$

in contrast to the Ramsey fringe height in the absence of a QND measurement: $\langle J_z \rangle = (N_A/2)\sin\varphi$. Therefore, a QND measurement reduces the clock phase sensitivity (given by the Ramsey signal slope $\mathrm{d}\phi/\mathrm{d}\varphi$) by a factor of $1 - \eta$. Tailoring the QND measurement strength induces squeezing and thus improves the signal-to-projection-noise ratio by $1/\xi$ in variance as given in equation (1).

We emphasize that atoms that have undergone spontaneous emissions into the $m_F \neq 0$ states do not take part in the clock rotations: due to the magnetic bias field the microwave radiation only couples the $|F = 3, m_F = 0\rangle$ to the $|F = 4, m_F = 0\rangle$ state. These atoms are, however, part of the entangled state as they carry some part of the information of the QND measurement outcome: only when these atoms are measured together with the $m_F = 0$ atoms in the second measurement is there no additional partition noise due to spontaneous emissions. It is therefore important that, in the absence of a phase shift ($\varphi = 0$), the rotation operator corresponding to our microwave clock pulse sequence commutes with J_z, i.e. the population difference ΔN is not changed.

3.2. Low phase noise microwave source

A projection noise limited atomic clock with $N_A = 10^5$ atoms can resolve atomic phase fluctuations as small as $\delta\varphi = 1/\sqrt{N_A} = 3\,\mathrm{mrad}$. This poses strict requirements on the phase noise of our microwave oscillator: during the interrogation time its phase has to be much more stable than $1/\sqrt{N_A}$ so that our clock performance is not limited by the oscillator. For an oscillator with a white phase noise spectrum and for a clock interrogation time of $T = 10\,\mu\mathrm{s}$, this translates into a required relative phase noise power density lower than $-100\,\mathrm{dBc\,Hz^{-1}}$ over a $100\,\mathrm{kHz}$ sideband next to the $9.192\,\mathrm{GHz}$ carrier. This is more than one order of magnitude smaller than the phase noise of the Agilent HP8341B microwave synthesizer used in [12].

A key step in the implementation of the clock sequence therefore was the construction of a low-noise synthesizer chain: a $9\,\mathrm{GHz}$ dielectric resonator oscillator (DRO-9.000-FR, Poseidon Scientific Instruments) with a phase noise of $-132\,\mathrm{dBc\,Hz^{-1}}$ at $100\,\mathrm{kHz}$ is phase locked to an oven-controlled $500\,\mathrm{MHz}$ quartz oscillator (OCXO) (MV87, Morion Inc.) within a bandwidth of $15\,\mathrm{kHz}$. The OCXO itself is slowly ($\approx 10\,\mathrm{Hz}$) locked to a GPS reference. A direct digital synthesis (DDS) board (Analog Devices AD9910) is clocked from the frequency doubled OCXO and produces a $192\,\mathrm{MHz}$ signal, which is mixed onto the DRO output; a microwave cavity resonator, with a $50\,\mathrm{MHz}$ width, filters out the upper $9.192\,\mathrm{GHz}$ sideband. By using the DDS to shape the microwave pulses, we control the microwave pulse duration with a precise timing in $4\,\mathrm{ns}$ steps and control the microwave phase digitally with a $2\pi \times 2^{-16}\,\mathrm{rad}$ resolution, allowing for complex and precise pulse sequences.
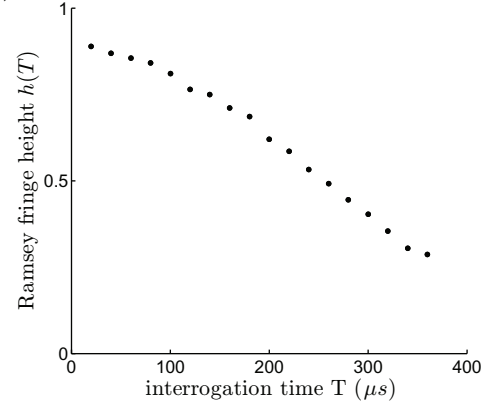
(a)
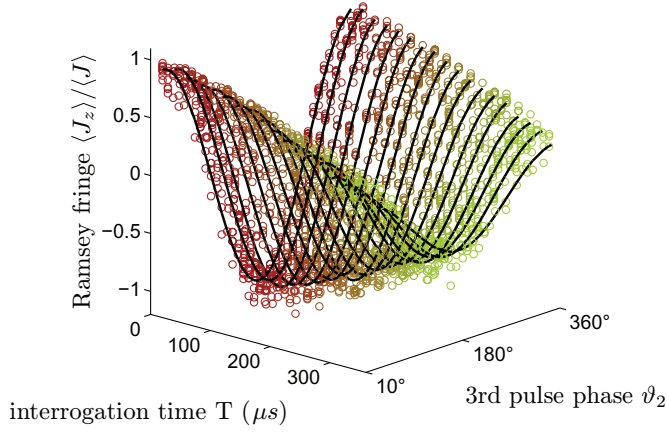
(b)

Figure 7. (a) Ramsey fringe for interrogation times ranging from $10\,\mu$s (red points) to $350\,\mu$s (green points). Solid lines: fits of the type $\langle J_z\rangle/\langle J\rangle = h(T)\cos\vartheta_2$ to the data. (b) Fringe contrast $h(T)$ derived from the fits in (a).

3.3. Ramsey fringe decay

We first operate our clock with the sequence described in figure 6, leaving out the first QND measurement. The phase ϑ_2 of the last microwave pulse is varied between $0°$ and $360°$. The microwave frequency is set to resonance (to within $10\,$Hz), so we expect $\langle J_z\rangle = (N_A/2)\cos\vartheta_2$. In figure 7, we plot the distribution of J_z-measurements normalized to $\langle J\rangle = N_A/2$, for different interrogation times T between 10 and $350\,\mu$s. The differential ac-Stark shift induced by the Gaussian dipole trap potential causes spatially inhomogeneous dephasing during the whole interrogation time T. This results in a decay of the Ramsey fringe contrast $h(T)$ (and therefore a decay of the clock phase sensitivity) as T increases, as shown in figure 7.

3.4. Ramsey sequence with squeezing

We implement the full EAR sequence described in figure 6 and keep the last microwave pulse phase $\vartheta_2 = 180°$. The noise contributions to the second QND measurement are shown in figure 8. With such a short interrogation time ($10\,\mu$s), only little classical noise is added to the second measurement, compared to the first measurement ($\mathrm{var}(\phi_1) \approx \mathrm{var}(\phi_2)$). We attribute this classical noise to microwave frequency noise and dipole trap intensity fluctuations.

Using the first weak measurement ϕ_1 to predict the outcome of the second measurement ϕ_2, we observe a metrologically relevant noise reduction of $\xi = -1.1\,$dB for 9×10^4 atoms. This gives us the signal-to-projection-noise ratio improvement that we gained by running our clock with an entangled atomic ensemble, compared to a standard clock operating with unentangled atoms (see figure 8). The experimentally observed squeezing is lower than the expected value $\xi_{\mathrm{lin}} = [(1-\eta)^2(1+\kappa^2)]^{-1} = -2.2\,$dB because of the extra classical noise in the second measurement ϕ_2.

Note that the obtained squeezing is different from the one shown in figure 4. Apart from the fact that the atom number used in the clock experiment is lower, the reduction of the spin squeezing can be explained by two experimental effects. Firstly, the atomic motion in the trap
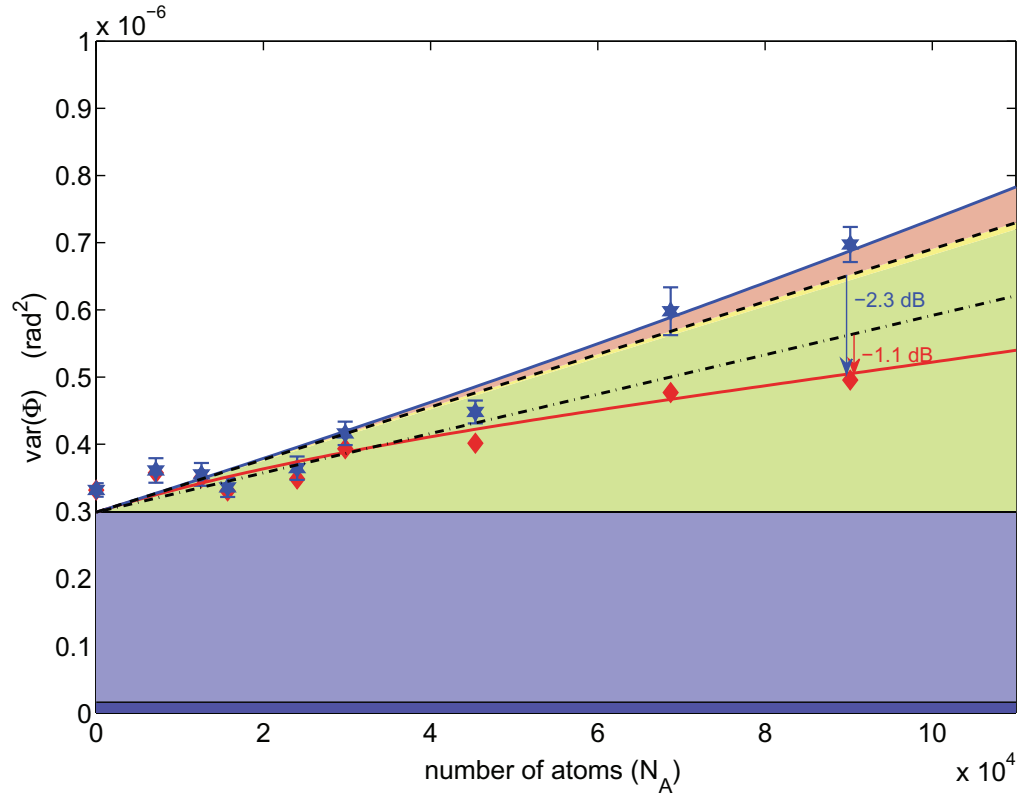
Figure 8. Noise contributions to the second measurement in the clock sequence, with an interrogation time of $T = 10\,\mu$s. The first measurement contains 7.1×10^6 photons and induces a Bloch vector shortening of 13.5%.

results in a decay of the correlations $\text{cov}(\phi_1, \phi_2)$ during the longer time interval between the two QND measurements ϕ_1 and ϕ_2 in the clock sequence. Secondly, in the Ramsey sequence, phase and frequency fluctuations between atoms and the microwave oscillator affect the ϕ_2 measurement to first order (cf equation (10)), whereas they only appear in second order in the simple squeezing sequence shown in figure 1.

The first QND measurement ϕ_1 also produces backaction anti-squeezing on the conjugate spin variable J_x. Classical fluctuations in relative intensities of the two probe colors lead to a fluctuating differential ac-Stark shift between the clock levels. This adds additional noise to J_x, so that the produced SSS is about 10 dB more noisy in the (anti-squeezed) J_x quadrature than a minimum uncertainty state. However, this excess noise does not affect the clock precision since we only perform J_z measurements.

3.5. Frequency noise measurements

The Ramsey sequence makes it possible to use an atomic ensemble either as a clock, where the frequency of an oscillator is locked to the transition frequency between the clock states $\nu = (E_\uparrow - E_\downarrow)/h$, or as a sensor, to measure perturbations of the energy difference between these levels. In our experiment, the atomic ensemble is sensitive to fluctuations of the frequency difference Δ between the cesium clock transition and the microwave oscillator.

The atomic transition frequency of 9 192 630 500 Hz as measured in our experiments has a systematic offset from the SI value of 9 192 631 770 Hz mainly for two reasons. Firstly, the bias field of ≈ 1 G causes a quadratic Zeeman shift of $+427$ Hz G^{-2} on the clock transition. Secondly, the trapping light produces a differential ac-Stark shift of the order of -1700 Hz averaged over the atoms within the probe beam. Noise in the phase evolution between the atoms and the microwave oscillator leads to added classical noise in the ϕ_2 measurement, which scales as N_A^2.

The frequency noise components that an atomic clock can detect are determined by the clock's cycle time t_c and the interrogation time T. Uncorrelated frequency fluctuations from cycle to cycle result in additional noise in the ϕ_2-measurement that scales as T^2 in variance. Phase noise between atoms and the microwave oscillator during the interrogation time T, however, can follow a different scaling behavior. Since we subtract the outcomes of successive MOT loading cycles, our clock is not sensitive to any frequency noise slower than $t_c = 5$ s.

3.6. Influence of classical noise on the clock performance

The quantum noise limited frequency sensitivity of an atomic clock improves with increasing interrogation time. However, achieving a higher frequency sensitivity makes our experiment more susceptible to classical noise. In order to evaluate the limitations of our proof-of-principle experiment, we vary the interrogation time T from 10 to 310 μs by steps of 20 μs, while keeping the atom number approximately constant at $N_A = 9 \times 10^4$. From the optical phase shift measurements ϕ_1 and ϕ_2, we can infer the atomic phase evolution by normalizing to the Ramsey fringe amplitude and define

$$\tilde{\varphi}_2 = \frac{\phi_2}{A(T)}, \quad \tilde{\varphi}_{21} = \frac{\phi_2 - \zeta \phi_1}{A(T)}, \tag{11}$$

where $A(T) = \chi (1 - \eta) h(T) N_A$ and $h(T)$ is the Ramsey fringe contrast shown in figure 7.

In figure 9, we plot the measured atomic phase noise variance var($\tilde{\varphi}_2$) and the conditionally reduced noise of the atomic phase var($\tilde{\varphi}_{21}$) as a function of the interrogation time T. Only in the first data point (corresponding to $T = 10$ μs) do we observe squeezing, i.e. the measured noise in $\tilde{\varphi}_{21}$ is lower than that of a traditionally operated atomic clock with an identical signal-to-projection-noise ratio (i.e. with an atom number of N_A/ξ_{lin}).

We observe a quadratic increase in the classical noise with T. This suggests that the detuning is roughly constant over the interrogation time, but varies from cycle to cycle. We attribute these fluctuations to both intensity drifts in the dipole trap and variations of the geometry of the atomic cloud. From the fit (solid green line) we infer $\sqrt{\text{var}(\Delta)} = 7.5$ Hz per cycle.

4. Conclusion

In summary, we have demonstrated the first EAR clock, following the proposal of [12]. We have implemented a modified Ramsey sequence in which the spin state is squeezed by means of a QND measurement. Squeezing results in a metrologically relevant reduction in the noise variance by -1.1 dB with 9×10^4 atoms, compared to a traditional atomic clock at the projection noise limit with the same number of atoms. The present experimental developments have been made possible by the introduction of a low phase noise microwave source.
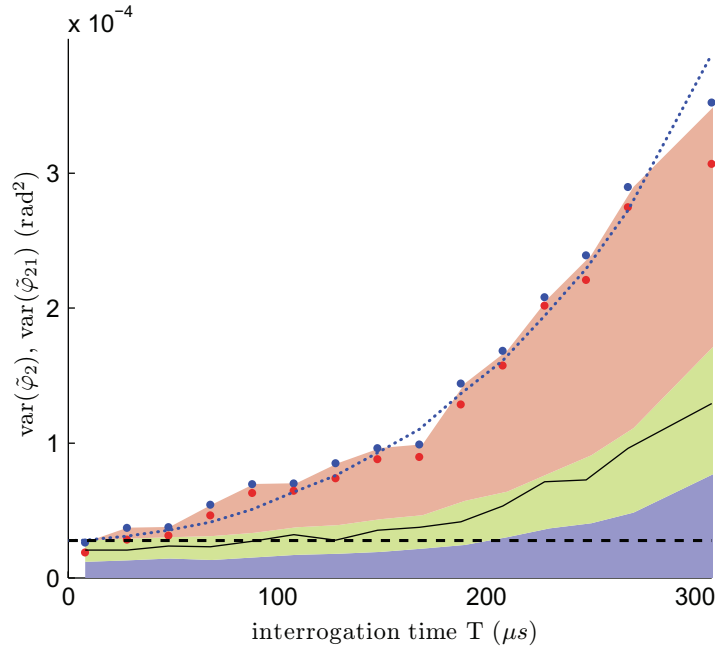
Figure 9. Contributions to the atomic phase noise as a function of the interrogation time T. Blue points: $\mathrm{var}(\tilde{\varphi}_2)$. Red points: $\mathrm{var}(\tilde{\varphi}_{21})$. For each interrogation time T, we determine the various noise contributions to $\mathrm{var}(\phi_2)$, as shown in figure 8. Using equation (11), we obtain the noise contributions to $\mathrm{var}(\tilde{\varphi}_2)$. The different contributions to $\mathrm{var}(\tilde{\varphi}_2)$ are the shot noise (blue area), projection noise (green area) and classical noise (red area). The dotted line is a quadratic fit to the classical noise contribution to $\mathrm{var}(\tilde{\varphi}_{21})$ (red area). The solid line shows the reduced projection noise, which would be obtainable in the absence of classical noise. The dashed line demarcates the area in which the Wineland criterion (cf equation (1)) is satisfied $\mathrm{var}(\tilde{\varphi}_{21}) < 1/N_A$, corresponding to the regime of metrologically relevant squeezing. In the absence of classical noise, the maximum interrogation time at which the Wineland criterion would be satisfied is given by the intersection between the dashed and solid lines at $T = 90\,\mu\mathrm{s}$.

The dual-color QND method implemented in this work is readily applicable to optical clocks as well. The idea of using QND measurements to generate entanglement and to improve the precision of a clock has drawn the attention of the ultra-precise-frequency-standards community [8, 13]. Besides, non-destructive measurements have been shown to drastically improve the duty cycle in a clock experiment, thereby reducing the Dick effect [13].

We have shown that, for the present proof-of-principle experiment, the improvement of the clock precision due to squeezing does not extend to interrogation times beyond $10\,\mu\mathrm{s}$. This is due to the inhomogeneous broadening on the hyperfine transition induced by the dipole trap, and the fact that large interrogation times make the clock more sensitive to light shifts induced by cloud-geometry and intensity fluctuations in the dipole trap. These issues could be circumvented by turning to systems for which there exists a magic wavelength, such as strontium [33, 34] or ytterbium [35]. For long interrogation times, the clock performance is also limited by the atomic motion, which can be counteracted by introducing a transverse optical lattice.

IOP Institute of Physics ✦ DEUTSCHE PHYSIKALISCHE GESELLSCHAFT

The figure of merit for the QND-induced spin squeezing is the resonant optical depth of the atomic ensemble. In the present experiment, the optical depth was limited to a value ≈ 10. Implementation of QND-based spin squeezing in state-of-the-art clocks will require solutions where high optical depth can be combined with low collisional broadening, such as optical lattices placed in a low-finesse optical cavity.

References

[1] Santarelli G, Laurent P, Lemonde P, Clairon A, Mann A G, Chang S, Luiten A N and Salomon C 1999 *Phys. Rev. Lett.* **82** 4619
[2] Wilpers G, Binnewies T, Degenhardt C, Sterr U, Helmcke J and Riehle F 2002 *Phys. Rev. Lett.* **89** 230801
[3] Ludlow A D *et al* 2008 *Science* **319** 1805
[4] Wineland D J, Bollinger J J, Itano W M, Moore F L and Heinzen D J 1992 *Phys. Rev.* A **46** R6797
[5] Huelga S F, Macchiavello C, Pellizzari T, Ekert A K, Plenio M B and Cirac J I 1997 *Phys. Rev. Lett.* **79** 3865
[6] Giovannetti V, Lloyd S and Maccone L 2004 *Science* **306** 1330
[7] André A, Sørensen A S and Lukin M D 2004 *Phys. Rev. Lett.* **92** 230801
[8] Meiser D, Ye J and Holland M J 2008 *New J. Phys.* **10** 073014
[9] Meyer V, Rowe M A, Kielpinski D, Sackett C A, Itano W M, Monroe C and Wineland D J 2001 *Phys. Rev. Lett.* **86** 5870
[10] Wasilewski W, Jensen K, Krauter H, Renema J, Balabas M V and Polzik E 2009 Quantum noise limited and entanglement-assisted magnetometry arXiv:0907.2453v3
[11] Koschorreck M, Napolitano M, Dubost B and Mitchell M W 2009 Measurement of spin projection noise in broadband atomic magnetometry arXiv:0911.4491v1
[12] Appel J, Windpassinger P J, Oblak D, Hoff U B and Kjaergaard N 2009 *Proc. Natl Acad. Sci.* **106** 10960
[13] Lodewyck J, Westergaard P G and Lemonde P 2009 *Phys. Rev.* A **79** 061401
[14] Itano W M, Bergquist J C, Bollinger J J, Gilligan J M, Heinzen D J, Moore F L, Raizen M G and Wineland D J 1993 *Phys. Rev.* A **47** 3554
[15] Sørensen A, Duan L-M, Cirac J I and Zoller P 2001 *Nature* **409** 63
[16] Estève J, Gross C, Weller A, Giovanazzi S and Oberthaler M K 2008 *Nature* **455** 1216
[17] Kuzmich A, Mølmer K and Polzik E S 1997 *Phys. Rev. Lett.* **79** 4782
[18] Hald J, Sørensen J L, Schori C and Polzik E S 1999 *Phys. Rev. Lett.* **83** 1319
[19] Appel J, Figueroa E, Korystov D, Lobino M and Lvovsky A I 2008 *Phys. Rev. Lett.* **100** 093602
[20] Honda K, Akamatsu D, Arikawa M, Yokoi Y, Akiba K, Nagatsuka S, Tanimura T, Furusawa A and Kozuma M 2008 *Phys. Rev. Lett.* **100** 093601
[21] Grangier P, Roch J.-F and Roger G 1991 *Phys. Rev. Lett.* **66** 1418
[22] Kuzmich A, Bigelow N P and Mandel L 1998 *Europhys. Lett.* **42** 481
[23] Kuzmich A, Mandel L and Bigelow N P 2000 *Phys. Rev. Lett.* **85** 1594
[24] Chaudhury S, Smith G A, Schulz K and Jessen P S 2006 *Phys. Rev. Lett.* **96** 043001
[25] Schleier-Smith M H, Leroux I D and Vuletić V *Phys. Rev. Lett.* **104** 073604
[26] Takano T, Fuyama M, Namiki R and Takahashi Y 2009 *Phys. Rev. Lett.* **102** 033601
[27] Julsgaard B, Kozhekin A and Polzik E S 2001 *Nature* **413** 400
[28] Saffman M, Oblak D, Appel J and Polzik E S 2009 *Phys. Rev.* A **79** 023831

[29] Windpassinger P J, Oblak D, Petrov P G, Kubasik M, Saffman M, Alzar C L G, Appel J, Müller J H, Kjærgaard N and Polzik E S 2008 *Phys. Rev. Lett.* **100** 103601

[30] Appel J, MacRae A and Lvovsky A I 2009 *Meas. Sci. Technol.* **20** 055302

[31] Windpassinger P J, Oblak D, Hoff U B, Louchet A, Appel J, Kjaergaard N and Polzik E S 2009 *J. Mod. Opt.* **56** 1993

[32] Oblak D, Appel J, Windpassinger P, Hoff U, Kjaergaard N and Polzik E 2008 *Eur. Phys. J.* D **50** 67

[33] Katori H, Takamoto M, Palchikov V G and Ovsiannikov V D 2003 *Phys. Rev. Lett.* **91** 173005

[34] Ye J, Kimble H J and Katori H 2008 *Science* **320** 1734

[35] Barber Z W *et al* 2008 *Phys. Rev. Lett.* **100** 103002